Response Under 37 CFR 1.116
Expedited Procedure
Examining Group 1631

B189

IN THE UNITED STATES PATENT AND TRADEMARK OFFICE

Examiner	:	Marjorie A. Moran
Group	:	1631
Applicants	:	MIHAIL N. KARPUSAS, JUSWINDER SINGH AND DAVID W. THOMAS
Application No.	:	09/180,209
Confirmation No.	:	6529
Filing Date	:	December 22, 1999
For	:	CRYSTALS OF FRAGMENTS OF CD40 LIGAND AND THEIR USE

Hon. Commissioner for Patents
P.O. Box 2327
Arlington, Virginia 22202

DECLARATION OF JUSWINDER SINGH
UNDER 37 C.F.R. § 1.132

I, JUSWINDER SINGH, hereby declare that:

1. I am one of the named inventors of the above-identified patent application.

2. I am an Associate Director, Structural Informatics, at Biogen, Inc., the assignee of the above-identified application. I have a Ph.D. degree in Structural Bioinformatics from the University of London. My CV is attached herewith at Tab A.

3. I have read the August 21, 2002 final Office Action in the above-identified application. I have also read claims 39, 42 and 43, as I understand them to have been pending at the time of the Action. I understand that the Action includes a rejection of claims 39, 42 and 43, relating to a computer for displaying a three dimensional representation of a binding site, or molecule or molecular complex of CD40

Express Mail Label
No. EV 045437269 US

ligand, under 35 U.S.C. § 103. Specifically, I understand that, in the Examiner's view, claims 39, 42 and 43 are unpatentable over Staley, Comp. Usage Mater. Educ. Proc. Symp., 113-122 (1985), abstract only ("Staley") in view of Peitsch, et al., International Immunity, 5: 233-238 (1993) ("Peitsch") because it would have been obvious to one skilled in the art at the time of the invention to display amino acid residues 115 to 260 of CD40L as the structure coordinates for CD40L were known from the Peitsch model. I have also read Staley and Peitsch. I also have read the amended claims for the-above identified application and understand them to be those attached herewith at Tab B.

4. I make this declaration to demonstrate that the Peitsch model is not an accurate model for human CD40L.

5. Peitsch relates to a three dimensional model of mouse CD40L based on the known crystal structure of human tumor necrosis factor α (TNFα). As discussed on page 233 of Peitsch (right column, first full paragraph, lines 13-14), mouse CD40L is only 23.2 and 25.7% identical with human and mouse TNFα, respectively. Given the low sequence similarity between TNFα (upon which the model was built) and mouse CD40L, the Peitsch model must be recognized as merely a speculative model of mouse CD40L.

6. In contrast to the Peitsch model of mouse CD40L, the crystal structure discussed in the above-identified application is of human CD40L. The human and mouse proteins are 78% homologous (see Spriggs, et al., J. Exp. Med., 176: 1543-1550 (1992) at page 1548, end of right column to beginning of left column, first full paragraph of the Discussion section, starting at line 9, attached herewith at Tab C). More importantly, as shown in Figure 1 (attached herewith at Tab D), residues 115 to 260 of human CD40L,

which include the residues corresponding to the binding site of amended claim 43 for CD40 in human CD40L, differ significantly from the corresponding residues of mouse CD40L. Hence, the Peitsch model would not be viewed as representative of the human CD40L structure to a high degree of accuracy because it is a model of mouse CD40L.

7. The Peitsch model does not provide an accurate structure of human CD40L; it especially does not provide an accurate structure of the binding site of human CD40L for the natural ligand, CD40. Due to the lack of accuracy, the Peitsch model would not be useful for structure-based drug design for human therapeutics. Structure-based drug design is an important and exciting means for obtaining drug candidates. A desire to perform such drug design for agonists or antagonists of human CD40L and the lack of appropriate structural model in the art provided incentive to obtain the crystal structure of human CD40L. Such a structural model is provided by the crystal structure disclosed in the above-identified patent application which serves as the source for the structure coordinates recited in the claims.

8. On pages 233-4 of Peitsch, Peitsch justified building a model of mouse CD40L from TNFα based on the structural similarity between human TNFα and TNFβ. Comparisons of the crystal structures of human TNFα and TNFβ using superposition of the Cα atoms of the core β-strand residues only yields a 0.61Å root mean square deviation (rmsd) (Eck, et al., J. Biol. Chem. 267: 2119-2122 (1992), attached herewith at Tab E), even though the two proteins share only a 30.6% sequence identity. Peitsch speculated that this structural conservation in the face of low sequence identity could extend to mouse CD40L modeled from human TNFα.

9. We have tested the accuracy of the Peitsch model experimentally by comparing it to the crystal structure set forth in the above-identified application. As shown below, there are significant structural differences between the two structures, confirming the inaccuracy of the Peitsch model as a model for human CD40L.

10. We performed an overlay between the binding site of CD40L for CD40 of the crystal structure model characterizing the three dimensional representation of amended claim 43 in the above-identified application and its equivalent in the Peitsch model. The binding site of the three dimensional representation of amended claim 43 of the present application is defined by structure coordinates of human CD40 ligand amino acids Ile127, Ser128, Glu129, Ala130, Ser131, Thr135, Ser136, Ala141, Glu142, Lys143, Gly144, Tyr145, Tyr146, Cys178, Asn180, Ser185, Gln186, Ala187, Pro188, Ile190, Ala191, Ser192, Ser197, Pro198, Gly199, Arg200, Phe201, Glu202, Arg203, Ile204, Arg207, Ala209, Thr211, Pro217, Cys218, Gly219, Gln220, Glu230, Leu231, Gln232, Asn240, Val241, Thr242, Asp243, Ser245, Val247, Ser248, His249, Gly250, Thr251, Gly252 and Phe253. These coordinates were compared to coordinates from the corresponding amino acid residues from the Peitsch mouse CD40L model. This backbone alignment between the Peitsch mouse model and the human CD40L crystal model disclosed in the present application shows a rmsd value of 2.8 Å. This should not be surprising, given that the Peitsch model is not for a structure of human CD40L. In addition, we performed an overlay between the backbones atoms of entire CD40L model from Peitsch and the crystal structure characterizing the three dimensional representation of a molecule of molecular complex of amended claim 42 of the instant application, and an overlay between backbone atoms of residues Lys143, Tyr145, Arg203 and Arg207 of

the crystal structure characterizing the three dimensional representation of a binding site for CD40 on CD40L of amended claim 39 and the corresponding amino acid residues of the Peitsch model. The backbone alignment between the Peitsch model and the crystal structure characterizing the three dimensional representation of a molecule of molecular complex of amended claim 42 of the instant application shows a rmsd value of 2.88 Å (Figure 2, attached herewith at Tab F). The backbone alignment of residues Lys143, Tyr145, Arg203 and Arg207 of the crystal structure characterizing the three dimensional representation of a binding site of amended claim 39 and the corresponding amino acid residues of the Peitsch model gives an rmsd value of 1.306 Å. The high rmsd values in these three alignments show that the Peitsch model is not an accurate or true model for the human CD40L structure characterizing the three dimensional representation of a molecule or molecular complex or a binding site of amended claims 39, 42 and 43.

11. Figure 2 shows a view of an overlay of the backbone atoms of the Peitsch model and the crystal structure characterizing the three dimensional representation produced by a computer of amended claim 42 of the above-identified application looking from the CD40 side on the CD40-CD40L binding interface. All the side chains that are closer than 5.0Å from the CD40 binding site in the crystal structure are shown in sticks while the backbones are drawn as lines.

12. In Figure 2, the Peitsch model (PDB accession code, 1cda) is in orange and the human CD40L crystal structure disclosed in the above-identified application (PDB accession code, 1aly) is in blue. While it is apparent from Figure 2 that the backbones of the Peitsch mouse CD40L model (the orange line) and the human CD40L crystal structure (the blue line) significantly differ or do not overlap over many

parts of the entire structure, the differences in the amino acid side chains from Peitsch mouse CD40L model (in orange stick) and the side chains of the human CD40L crystal model (in blue stick) in the binding site are striking. Little overlap exists between the side chains within 5Å of the CD40 binding site in the Peitsch mouse CD40L model and the human CD40L crystal structure.

13. In summary, Peitsch relates to a three dimensional model of mouse CD40L based on the known crystal structure of the human tumor necrosis factor α (TNFα). Comparison of the Peitsch model with the crystal structure of human CD40L disclosed in the above-identified application shows significant structural differences between the two structures, and illustrates the inaccuracy of Peitsch's model as a model for human CD40L. Backbone alignments between the Peitsch model and the CD40L crystal structure as recited in the three dimensional representations produced by a computer of amended claims 42 and 43 show a large root mean square deviation (rmsd) value of at least 2.8 Å, while backbone alignment between the Peitsch model and the CD40L crystal structure as recited in the three dimensional representations produced by a computer of amended claim 39 show a root mean square deviation value greater than 1.0 Å. In addition, inspection of the side chains in the CD40 binding site reveals little overlap between Peitsch's speculative mouse model and the human crystal structure.

14. If the Peitsch model were combined with the computer of Staley, the resulting combination would not yield or suggest the computers claimed in this application, because Peitsch does not disclose or suggest the recited three dimensional representations of human CD40L.

15. I declare further that all statements made herein of my own knowledge are true and that all statements made herein on information and belief are believed to be true; and further, that these statements were made with the knowledge that willful false statements and the like so made are punishable by fine or imprisonment, or both, under Section 1001, Title 18, United States Code, and that such willful false statements may jeopardize the validity of this application and any patent issuing thereon.

Date: 2/7/2003

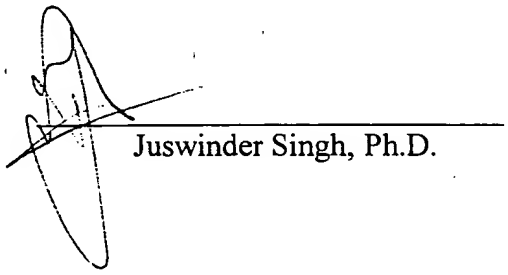

Juswinder Singh, Ph.D.

APPENDIX A

JUSWINDER SINGH

Address
94 Heritage Avenue
Ashland
MA01721
Tel:6176792027

Visa Status: U.S. Permanent Resident

Work Experience

Oct96 – Present Associate Director
Structural Informatics
Biogen Inc.

Oct94 – Oct96 Senior Scientist
Structural Informatics
Biogen Inc.

Oct91 – Oct94 Senior Scientist,
CADD Group,
Parke-Davis Research

Education

1981-1984 Department of Biochemistry
University of Sussex, England
B.Sc. Biochemistry (First Class Honors)

1984-1987 PhD. In Structural Bioinformatics
Joint collaboration of Pfizer Inc. And University of London
Supervised by Sir . T.L. Blundell F.R.S. (Cambridge University), Prof. Janet Thornton F.R.S. (University College London) and Dr. S.Campbell (V.P. of Discovery Research, Pfizer, Sandwich, Kent)

Post-Doctoral Experience

May87 - Sept91 Post-Doctoral Research Scientist
Biomolecular Structure and Modeling Group
University College London
Supervisor : Prof. Janet Thornton F.R.S.

Publications

1. **Singh J**, Thornton JM. "The Geometries of Interacting Phenylalanine Rings in Proteins," FEBS Lett 1985;191:1-6.

2. Blundell TL, **Singh J**, Thornton JM, BurleySK, PetskoGA. "Aromatic Interactions," Science 1986;1005:234

3. **Singh J**, Thornton JM, Snarey M, Campbell SF. "The Geometries of Interacting Arginine-Carboxyls in Proteins," FEBS Lett 1987;224:161-71.

4. Blundell, TL, Elliott, G., Gardner, SP, Hubbard, T., Islam, S., Johnson, M., Mantafounis, D., Murray-Rust, P., Overington, J., Pitts, JE, Sali, A., Sibanda, BL., **Singh, J.,** Sternberg, MJE, Sutcliffe, MJ., Thornton, JM., Travers, "Protein Engineering and Design", 1989 P. Phil. Trans. R. Soc. Lond. B324, 447-460

5. Thornton JM, **Singh J**, Campbell SF, Blundell TL. "Protein-Protein Recognition via Side Chain-Side Chain Interactions," Biochemical Society Transactions 1988;16:927-93.

6. **Singh J**, Thornton JM. "SIRIUS-An Automated Method for Analyzing Protein Interactions," JMol Biol 1990;211:595-615

7. **Singh J**, Thornton JM, Saldanha JW. "A Novel Method for the Modelling of Ligands to their Receptors," Protein Engineering 1991;4:251-61.

8. Hunter C, **Singh J.** and Thornton, J.M., "Energetics of Aromatic-Aromatic Interactions," JMol Biol 1991;218, 837-849

9. Mitchell J, Thornton JM, **Singh J**. and Price, S.L., "Towards Understanding the Energetics of Arginine-Carboxylate Pairs in Proteins," JMol Biol 1992; **226**, 251-264

10. **Singh J**, Nandi CL, Thornton JM. "Atomic Environments of Arginine Side Chains in Proteins," Protein Engineering 1993, **6**, 247-259

11. **Singh, J.** "Comparative Analysis of the Ser/Thr and Tyr Protein Kinases : Proposed model for the catalytic domain of the epidermal growth factor receptor", Protein Engineering, 1994, 7, 849-858

12. Mitchell J.B , Nandi, C.L., Price S, **Singh J**, Snarey M and Thornton, J.M " A Comparison of Three Theoretical Approaches to the Study of Side Chain Interactions in Proteins " J. Chem. Soc. Faraday Trans., 1993, **89**, 2619-2630

13. Mitchell, J.B., Thornton, J.M., Price, S.L., McDonald, I., Nandi, C.L. and **Singh, J**. "Aromatic-amino hydrogen-bonds", Nature, 1993,366,413 (Correspondance)

14. Mahdevan, D., Thanki, N., **Singh, J.**, Wang, A.C., McPhee, P., Zangrilli, D., Wang, L., Gurerrero, C., Humblet, C., Saldanha, J., and Haske, T. "Structural Studies on the PH domains of Dbl, SOS1, IRS-1 and □ARK-1 and their differential binding to G□□ subunits", 1995, Biochemistry,34, 9111-9117

15. Zhu, G., Decker, S.J., Maclean, D., McNamara, D.J., **Singh, J.**, Sawyer, T.K. and Saltiel, A.R., 1994, "Sequence specificity in the recognition of the epidermal growth factor receptor by the abl Src homology 2 domain", Oncogene, 9,1379-1385

16. Fry, D.W., McMichael, A., **Singh, J.**, Dobrusin, E.M., and McNamara, D., (1994) "Design of a potent peptide inhibitor of the epidermal growth factor receptor tyrosine kinase utilizing sequences based on the natural phosphorylation sites of phospholipase C□1", Peptides, 15,951-957

17. Evans, R.W., Crawley, J.B., Garratt, R.C., Grossmann, J.G., Neu, M., Aitken, A., Patel, K.J., Meilak, A., Wong, C., **Singh, J.**, Bomford, A. and Husnain, S.S. "Characterisation and structural analysis of a functional human serum transferrin variant and its implications for receptor recognition", 1994, Biochemistry, 33, 12512-12520

18. Maclean, D., Thieme-Sefler, A.M., Zhu, G., Decker, S.J., Saltiel, A.R., **Singh, J.**, McNamara, D., Dobrusin, E.M. and Sawyer, T.K. "Differentiation of peptide molecular recognition by phospholipase C-1□ Src homology-2 domain and a mutant phosphatase PTP1b^{C215S}", 1995, Protein Science, 4, 13-20

19. Narasimhan, L., **Singh, J.**, Humblet, C., Guruprasad, K. and Blundell, T.L. "Snail and Spider toxins share similar structure and 'cystine pattern'", 1995, Nature Structural Biology, 1, 850-852

20. Shahripour, A., Plummer, M.S., Lunney, E.A., Vara Prasad J.V.N., **Singh, J.**, Para, K.S., Stankovic, C.J., Eaton, S.R., Rubin, J.R., Pavlovsky, A.G., Humblet, C., Fergus, J.H., Marks, J.S, Decker, S.J., Herrera, R., Hubbell, S., Saltiel, A.R., and Sawyer, T.K. (1995) "Novel phosphotyrosine and hydrophobic D-amino acid replacements in the design of peptide ligands for pp60^{src} SH2 domain", Peptides: Chemistry, Structure and Biology, 394-396

21. Plummer, M.S., Lunney, E.A., Para, K.S., Vara Prasad J.V.N., Shahripour A., **Singh, J.**, Stankovic, C.J., Humblet, C., Fergus, J.H., Marks, J.S., and Sawyer, T.K. (1995) "Hydrophobic D-amino acids in the design of peptide ligands for the pp60src SH2 domain", Drug Design and Discovery, 13,75-81

22. Laskwoski, R.A., Thornton, J., Humblet, C. and **Singh, J.** (1996) "XSITE: Use of empirically derived atomic packing preferences to identify favourable interaction regions in the binding sites of proteins',J. Mol. Biol., 259, 175-201

23. **Singh, J.**, Fry, D., Dobrusin, E., Whitty, A., Haske, T. and McNamara, D. (1997) "Structure-Based Design of a potent, selective and irreversible inhibitor of the erbB Receptor subfamily of Protein Tyrosine Kinases", J. Med. Chem, 40, 1130-1135

24. Wallace, A., Laskowski, R.A., **Singh, J.** and Thornton, J. (1996) 'Molecular Recognition by proteins:protein-ligand interactions from a structural perspective", Biochemical Society Transactions, 24, 280-284

25. **Singh,J** et al. (1998) 'The Role of Polar Interactions in the Molecular Recognition of CD40L with its counter-receptor CD40", Protein Science, 7:1124-1135

26. Saldanha, J., **Singh, J.** and Mahadevan, M. (1998) 'Frizzled-like Cysteine-Rich Domain in the Extracellular Region of Developmental Tyrosine Kinases', 7, Protein Science, 1632-1635

27. Gotwals, P., Chi-Rosso, G., Ryan, S.T., Sizing, I., Zafari, M., Benjamin, C., **Singh, J.**, Venyaminov, S.Y., Pepinsky, R.B. and Koteliansky, 1999, 'Divalent cations stabilize the a4b1 Integrin I domain', Biochemistry, 38, 8280-8288

28. **Singh, J**, van Vlijmen, H., Lee, WC, Liao, Y., Lin, KC, Ateeq, H., Cuervo. H., Zimmerman, C., Hammond, C., Karpusas, M., Palmer, R., Chattopadhyay, T., and Adams, SP 2002 J. Computer-Aided Molecular Design, "3D-QSAR (COMFA) of a series of potent and highly selective VLA4 Antagonists", 16, 201-211

29. **Singh, J.,** van Vlijmen, H., Liao, Y., Lee, WC, Cornebise, M., Harris, M., Shu, I., Gill, A., Cuervo, J., Abraham, WM, and Adams, SP 2002 "Identification of potent and novel a4b1 antagonists using in silico screening", J. Med. Chem., 45:2988-2993

BOOKS CHAPTERS

30. **Singh J**, Nandi L, Thornton JM. "Towards Understanding How Side Chains Pack in Proteins" 1991, in "Molecular Conformations and Biological Interactions", eds., Balaram P. And Ramaseshan S., Bangalore, 1-18

31. Thornton JM, Sibanda BL, Wilmot CM and **Singh J**. "Patterns in Protein Sequence and Structure" Springer Series in Biophysics, Taylor WR, Springer-VerlagHD (eds). 1991; Volume6.

BOOKS

32. **Singh J** and Thornton JM. "An Atlas of Side Chain Packing in Proteins," Volumes I and II, Oxford University Press, 1992, ISBN 0-19-0963302-9.

APPENDIX B

B189 - AMENDED CLAIMS

39. (Thrice Amended) A computer for producing a three dimensional representation of a binding site for CD40 defined by structure coordinates of human CD40 ligand amino acids Lys143, Arg203, Arg207 and Tyr145, which correspond to residues 28, 88, 92 and 30, respectively, of SEQ ID NO: 3, according to Table 1;

wherein said computer comprises:

(a) a computer program with instructions to produce said three dimensional representation;

(b) a computer-readable data storage medium comprising a data storage material encoded with computer-readable data, wherein said data comprises the structure coordinates of human CD40 ligand amino acids Lys143, Arg203, Arg207 and Tyr145, which correspond to residues 28, 88, 92 and 30, respectively, of SEQ ID NO: 3, according to Table 1; and

(c) a computer screen for displaying said three dimensional representation.

42. (Twice Amended) A computer for producing a three dimensional representation of a molecule or a molecular complex defined by the structure coordinates of all the human CD40 ligand amino acids according to Table 1; wherein said computer comprises:

(a) a computer program with instructions to produce said three dimensional representation;

(b) a computer-readable data storage medium comprising a data storage material encoded with computer-readable data, wherein said data comprises the structure coordinates of all the human CD40 ligand amino acids according to Table 1; and

(c) a computer screen for displaying said three dimensional representation.

43. (Amended) A computer for producing a three dimensional representation of a binding site for CD40 defined by structure coordinates of human CD40 ligand amino acids Ile127, Ser128, Glu129, Ala130, Ser131, Thr135, Ser136, Ala141, Glu142, Lys143, Gly144, Tyr145, Tyr146, Cys178, Asn180, Ser185, Gln186, Ala187, Pro188, Ile190, Ala191, Ser192, Ser197, Pro198, Gly199, Arg200, Phe201, Glu202, Arg203, Ile204, Arg207, Ala209, Thr211, Pro217, Cys218, Gly219, Gln220, Glu230, Leu231, Gln232, Asn240, Val241, Thr242, Asp243, Ser245, Val247, Ser248, His249, Gly250, Thr251, Gly252 and Phe253, which correspond to residues 12, 13, 14, 15, 16, 20, 21, 26, 27, 28, 29, 30, 31, 63, 65, 70, 71, 72, 73, 75, 76, 77, 82, 83, 84, 85, 86, 87, 88, 89, 92, 94, 96, 102, 103, 104, 105, 115, 116, 117, 125, 126, 127, 128, 130, 132, 133, 134, 135, 136, 137, and 138, respectively, of SEQ ID NO: 3, according to Table 1;

wherein said computer comprises:

(a) a computer program with instructions to produce said three dimensional representation;

(b) a computer-readable data storage medium comprising a data storage material encoded with computer-readable data, wherein said data comprises the structure coordinates of human CD40 ligand amino acids Ile127, Ser128, Glu129, Ala130, Ser131, Thr135, Ser136, Ala141, Glu142, Lys143, Gly144, Tyr145, Tyr146, Cys178, Asn180, Ser185, Gln186, Ala187, Pro188, Ile190, Ala191, Ser192, Ser197, Pro198, Gly199, Arg200, Phe201, Glu202, Arg203, Ile204, Arg207, Ala209, Thr211, Pro217, Cys218, Gly219, Gln220, Glu230, Leu231, Gln232, Asn240, Val241, Thr242, Asp243, Ser245, Val247, Ser248, His249, Gly250, Thr251, Gly252 and Phe253, which correspond to residues 12, 13, 14, 15, 16, 20, 21, 26, 27, 28, 29, 30, 31, 63, 65, 70, 71, 72, 73, 75, 76, 77, 82, 83, 84, 85, 86, 87, 88, 89, 92, 94, 96, 102, 103, 104, 105, 115, 116, 117, 125, 126, 127, 128, 130, 132, 133, 134, 135, 136, 137, and 138, respectively, of SEQ ID NO: 3, according to Table 1; and

(c) a computer screen for displaying said three dimensional representation.

APPENDIX C

Recombinant Human CD40 Ligand Stimulates B Cell Proliferation and Immunoglobulin E Secretion

By Melanie K. Spriggs,* Richard J. Armitage,‡ Laura Strockbine,* Ky N. Clifford,‡ Brian M. Macduff,‡, Timothy A. Sato,‡ Charles R. Maliszewski,‡ and William C. Fanslow‡

*From the Departments of *Molecular Biology and ‡Immunology, Immunex Research and Development Corporation, Seattle, Washington 98101*

Summary

Signaling through the cell surface molecule, CD40, is known to play an important role in the proliferation and differentiation of B lymphocytes. Using the thymoma cell line EL4, we recently identified and cloned a cDNA encoding a murine ligand for the CD40 molecule (mCD40-L) and showed that it has biological activity in vitro. A cDNA encoding a human homologue of the mCD40-L was isolated using crosshybridization techniques from an activated peripheral blood T cell library. The predicted amino acid sequence indicates that this human ligand for CD40 (hCD40-L) is a 261 amino acid type II membrane protein that exhibits 78% amino acid identity with its murine counterpart. Northern blot and FACS® analyses suggest that the hCD40-L is restricted in its expression to T lymphocytes, and that it is most abundant on the $CD4^+$ T cell subpopulation. Cells transfected with hCD40-L caused the proliferation of human tonsil B cells in the absence of costimuli and, in the presence of interleukin 4, induced immunoglobulin E secretion from purified human B cells. A comparison of the efficacy of the hCD40-L and mCD40-L in these assays is presented.

CD40 is a cell surface protein expressed on B lymphocytes, follicular dendritic cells, normal epithelium, and some epithelial carcinomas. The predicted amino acid sequence for CD40 indicates that it is a member of the recently described TNF receptor family of proteins (1–3). This family includes such molecules as the low affinity receptor for nerve growth factor, both forms of TNF receptors, CD27, OX40, and the Hodgkin's lymphoma marker CD30 (3, 4). In addition to structural homology to known cytokine receptors, functional effects in B cells have been shown to be mediated through mAbs directed against CD40. These effects include short- and long-term proliferation (5–7), differentiation (8, 9), induction of intercellular adhesion (10, 11), and tyrosine phosphorylation of a series of intracellular proteins (12). Furthermore, germinal center centrocytes are prevented from undergoing apoptosis when activated through their antigen receptors and by CD40 mAb (13). Taken together, these data strongly suggested that CD40 was the receptor for an unknown ligand.

Recently, we reported the molecular cloning of a ligand for CD40 from the murine thymoma cell line EL-4, and showed that this ligand was biologically active on primary B lymphocytes (14). Cells transfected with mCD40-L could induce the proliferation of murine and human B cells in the absence of costimuli. In this paper, we detail the cloning of a human homologue of the ligand for CD40; describe the relationship of the nucleotide and predicted amino acid sequences of the hCD40-L with those of the mCD40-L; examine the cellular distribution of the hCD40-L by Northern blot analysis and cell surface expression; compare the proliferative activity of both the hCD40-L and mCD40-L on human tonsillar and murine splenic B cells in the presence and absence of costimuli; and evaluate the ability of the two ligands to induce IgE secretion from IL-4–activated B cells.

Materials and Methods

Cell Separation. PBMC were purified from healthy donors by centrifugation over Histopaque® (Sigma Chemical Co., St. Louis, MO). Peripheral blood T cells (PB T)[1] were then purified by rosetting with 2-aminoethylisothiouronium bromide (AET)-treated SRBC and further centrifugation over Histopaque®. Contaminating monocytes were removed by plastic adherence for 1 h at 37°C. The resulting T cell preparations were always >98% $CD3^+$, as determined by flow cytometric analysis (FACScan®, Becton Dickinson & Co., Mountain View, CA). Tonsillar tissue was gently teased and the resulting cell suspension centrifuged over Histopaque®. T cells were purified as described for PB T cells. Purification of B cells was achieved by removal of cells rosetting with AET-treated SRBC and treatment of the remaining cells with B cell lympho-

[1] *Abbreviations used in this paper:* AET, aminoethylisothiouronium bromide; FBS, fetal bovine serum; PB T, peripheral blood T cells.

 J. Exp. Med. © The Rockefeller University Press • 0022-1007/92/12/1543/08 $2.00
Volume 176 December 1992 1543–1550

kwik (One Lambda Inc., Los Angeles, CA) for 1 h at 37°C to lyse contaminating non-B cells. The resultant B cell preparations were >96% $CD20^+$ as determined by flow cytometry. Murine splenic B cells were isolated using anti-T cell antibody and complement, followed by passage over Sephadex G-10 (Pharmacia Fine Chemicals, Piscataway, NJ) to remove adherent cells. B cells were then positively selected by panning on plates coated with 5 μg/ml goat anti-mouse IgM (Southern Biotechnology Associates, Birmingham, AL). Isolated cells were >95% surface IgM^+ as determined by flow cytometry.

Reagents. Murine and human recombinant IL-4 were purified from yeast supernatant as previously described (15). The 57-kD gene product of the extracellular domain of human CD40 fused to the Fc region of human IgG1 (CD40.Fc) was expressed, purified, and labeled with biotin-X-nonhydroxy succinimide (NHS; Calbiochem Corp., La Jolla, CA) as previously described (16). CV1/EBNA cells transfected with plasmids containing the hCD40-L or mCD40-L (see below) as described (14, 17), were cultured for 3 d on 10-cm petri dishes, removed and fixed with 1% paraformaldehyde for 10 min at 4°C, and washed extensively in culture medium before their use in biological assays.

Culture Conditions. For the preparation of RNA, PB T cells were activated for 20 h with immobilized CD3 mAb. Tonsil T cells were activated for 20 h with 10 ng/ml PMA and 1 μg/ml Con A. For proliferation assays, purified B cells (10^5/well) were cultured in triplicate with a titration of CV1/EBNA cells expressing human or murine CD40 ligand in flat-bottomed 96-well microtiter plates in 200 μl RPMI in a humidified atmosphere of 10% CO_2. For the proliferation of murine B cells, medium was supplemented with 5% heat-inactivated fetal bovine serum (FBS), 1 mM sodium pyruvate, 0.1 mM nonessential amino acids, 100 U/ml penicillin, 100 μg/ml streptomycin, 2 mM L-glutamine, and 50 μM 2-ME. For human B cells, medium was supplemented with 10% FBS, 100 U/ml penicillin, and 100 μg/ml streptomycin. Wells were pulsed with 2 μCi [^{3}H]thymidine (25 Ci/mmol) for the final 8 h of culture, cells were harvested, and incorporated cpm was determined by tritium-sensitive avalanche gas ionization detection on a beta counter (Matrix 96 Direct; Packard Instrument Co., Inc., Meriden, CT). Cultures for the determination of murine IgE secretion were performed as described for murine B cell proliferation assays but in supplemented RPMI 1640 containing 20% FBS. Culture conditions for the determination of human IgE were basically as described for human B cell proliferation assays but were conducted in round-bottomed 96-well microtiter plates. IgE levels in culture supernatants were determined by ELISA and were sensitive to 100 pg/ml and 4 ng/ml of human and murine IgE, respectively.

Flow Cytometric Analysis. Purified human PB T cells (10^6/ml) were cultured with 10 μg/ml immobilized OKT3 (CD3, American Type Culture Collection) mAb in the presence or absence of 10 ng/ml PMA for the times indicated. Cells were harvested and preincubated with 100 μg/ml human IgG1 in PBS plus 0.02% NaN_3 for 30 min at 4°C, to prevent nonspecific binding of staining reagents. Surface expression of CD40-L was determined by staining with 5 μg/ml biotinylated CD40.Fc for 30 min at 4°C. Cells were washed twice with PBS plus 0.02% NaN_3 and incubated for 30 min longer at 4°C with streptavidin-PE diluted 1:5 in PBS plus 0.02% NaN_3 and then analyzed using a FACScan® (Becton Dickinson & Co.). A minimum of 5,000 cells were analyzed for each sample.

cDNA Library Construction. Pooled human PB T were isolated from normal donors and cultured in 10 ng/ml IL-2 for 6 d followed by stimulation with 10 ng/ml PMA and 1 μg/ml Con A for 8 h. Polyadenylated RNA was used as a template to construct a random primed cDNA library using a cDNA synthesis kit (Amersham Corp., Arlington Heights, IL). cDNA was adaptored using EcoRI linkers and cloned into a λgtII vector (Stratagene Inc., La Jolla, CA). The library was screened with a ^{32}P-labeled mCD40-L riboprobe which was generated using SP6 polymerase (Promega Corp., Madison, WI) according to the supplier's protocol. This probe corresponds to the complete coding region of the mCD40-L gene, and was hybridized to the λgt11 library at 55°C in Stark's solution followed by washing in 2 × SSC 0.1% SDS at 63°C.

Transient Expression of hCD40-L in Mammalian Cells. The coding region of the hCD40-L was cloned into the mammalian expression vector pDC302 (17); DEAE transfections were performed in COS cells as described (18). Alternatively, pDC302 expression vector carrying the hCD40-L gene was cotransfected with the plasmid pSV3neo (19) using DEAE dextran into CV-1 EBNA cells (18).

Northern Blot Analysis. Northern blots were prepared essentially as described (20). Hybridization was performed in Stark's solution at 63°C followed by several washings in 0.2 × SSC, 1% SDS at 55°C. Blots were exposed for 1–3 d at −70°C.

Radiolabeling and Immunoprecipitations. COS cells expressing the hCD40-L protein or PB T cells cultured with immobilized CD3 as described for 3 h were radiolabeled with 100 μCi/ml ^{35}S Translabel (ICN Biomedicals, Inc., Irvine, CA) for 2–3 h. Cells were lysed in PBS containing 1% Triton X-100 and clarified at 10,000 *g* for 30 min. Lysates were incubated with purified CD40.Fc protein (1 μg/ml) for 30 min followed by the addition of protein A-Sepharose. After extensive washing, pellets were resuspended in sample buffer in the presence or absence of β-ME and analyzed by PAGE.

Results

Characterization of the hCD40-L cDNA Clone. A ^{32}P-labeled riboprobe corresponding to the coding region of the mCD40-L was used to screen a stimulated human PB T library under reduced stringency (see Materials and Methods). This resulted in the isolation of a 1,803-bp cDNA that contained the complete coding region of the hCD40-L. This clone contained a single open reading frame that could encode a polypeptide of 261 amino acids, a 45-bp 5′ noncoding region, and 975 bp of 3′ noncoding sequences which included a poly(A) tail. The predicted amino acid sequence of the hCD40-L and an alignment with the CD40-L is shown in Fig. 1. Like the mCD40-L, the hCD40-L is a type II membrane protein with a short 22-amino acid NH_2-terminal cytoplasmic domain followed by a 24-amino acid hydrophobic signal anchor region. The hCD40-L has a 215-amino acid COOH-terminal extracellular domain compared to 214 amino acids in the mCD40-L and five cysteine residues compared to four in the murine ligand. There is an N-linked glycosylation site in the extracellular domain that is conserved between the human and murine ligands, and an additional, but likely not utilized, glycosylation site in the cytoplasmic domain of hCD40-L. The two sequences exhibit 78% amino acid identity overall. More specifically, there is 81% amino acid identity between the cytoplasmic domains, 96% between the transmembrane regions, and 75% between the extracellular domains.

Expression and Immunoprecipitation of Recombinant hCD40-L. Oligonucleotide primers designed to include incompatible restriction sites were used in a PCR reaction to amplify

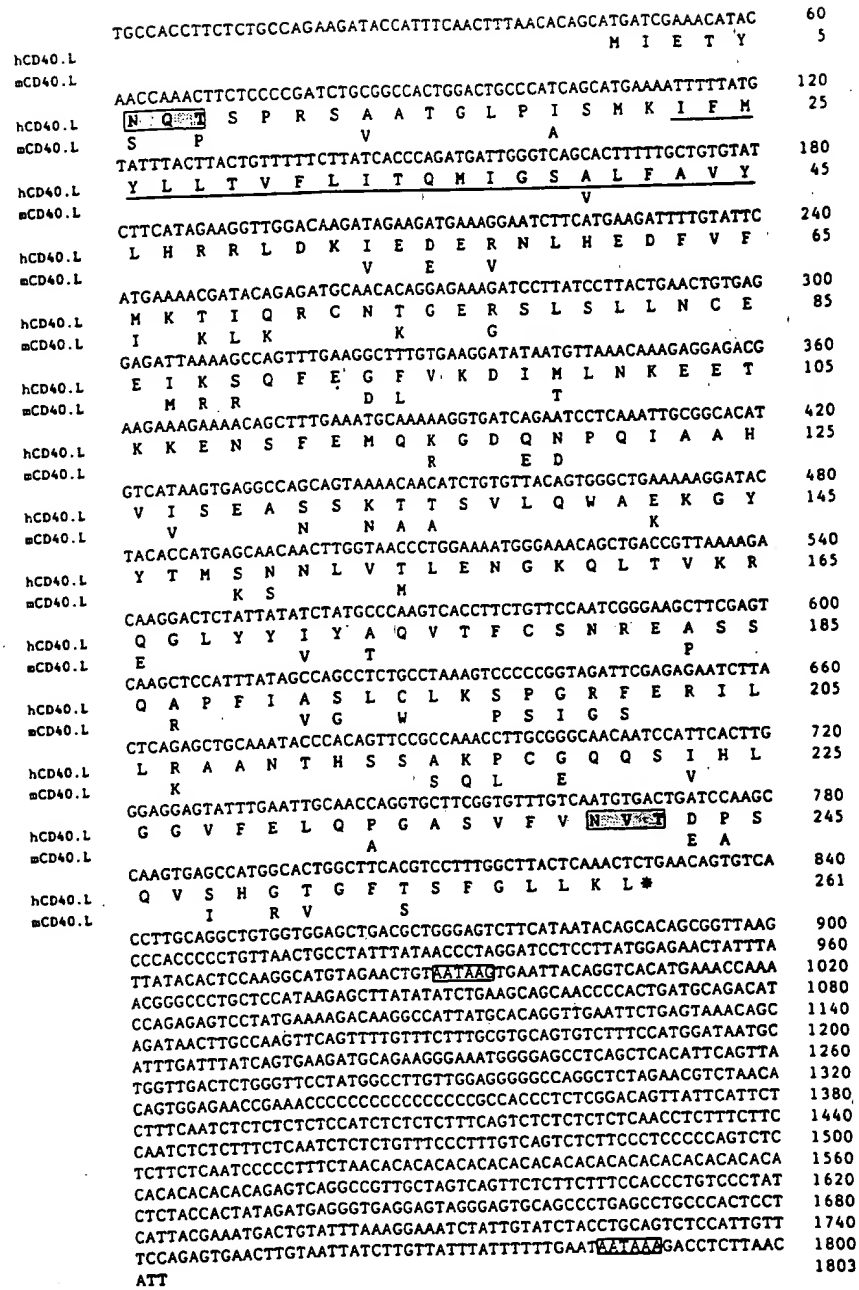

Figure 1. Nucleotide sequence exclusive of poly(A) of a cDNA encoding the hCD40-L protein (Genbank accession no. X67878). The predicted amino acid sequence of hCD40-L is given and compared with that of mCD40-L. Amino acid differences are indicated. The putative NH_2-terminal signal/anchor sequence is underlined, and potential N-linked glycosylation sites are shaded. A consensus sequence for addition of poly(A) is located at position 1784 (*boxed*), and a possible alternative poly(A) site occurs at position 989 (boxed).

the coding region of the hCD40-L gene. After digestion with the appropriate enzymes, the resulting PCR product was subcloned into a mammalian expression vector. Sequence analysis of the coding region insert confirmed that no nucleotide changes had occurred as a result of the PCR amplification. This plasmid was then used to transfect COS cells. The resulting recombinant hCD40-L was compared with the hCD40-L expressed on stimulated human PB T cells by metabolic labeling and precipitation using a previously described soluble CD40.Fc chimeric molecule (16). The results of this experiment are shown in Fig. 2. Immunoprecipitates electrophoresed under reducing conditions (lane *b*) indicate an apparent M_r of 33–35 kD for the recombinant hCD40-L. This protein comigrates with the hCD40-L protein derived from CD3 mAb-stimulated PB T cells (lane *d*). Immunoprecipitates electrophoresed under nonreducing conditions are essentially indistinguishable (data not shown), suggesting that the hCD40-L does not dimerize through disulphide bonding. A larger band (~ 69 kD) is present in the samples from stimulated PB T cells (lane *d*) or cells transfected with the hCD40-L (lane *b*), but not in control samples (lanes *c* and *e*). We addressed the possibility that this band might be due to oligomerization of the ligand through noncovalent bond formation by electrophoresing precipitated samples on polyacrylamide gels containing 7 M urea in the presence and absence of reducing agents. When these experiments are performed,

the results are similar to those in Fig. 2 (data not shown). Thus, the exact nature of the higher molecular weight material is still unclear, but it is not likely to be a simple oligomer of the hCD40-L.

Characterization of hCD40-L Expression by Northern Blot Analysis. Previously, we reported that mCD40-L mRNA was induced in T cells activated with CD3 mAb (14). We examined purified human PB T and tonsil T cells for their expression of hCD40-L mRNA in response to various stimuli. Total RNA from PB T cells activated with CD3 mAb, or tonsil T cells stimulated with PMA and Con A, was analyzed on Northern blots using a ^{32}P-labeled antisense RNA probe (Fig. 3). No detectable hCD40-L was present in unstimulated PB T or tonsil T cell total RNA, but was inducible under both stimulation conditions. It is interesting that both PB T and tonsil T cells express what appear to be two hCD40-L-specific mRNAs. The larger band is typically more prominent than the smaller band and appears to be ~2,000 bases in length, comparable to the size of the single mCD40-L mRNA seen in murine T cells. The exact nature of the smaller band is unclear. PCR experiments (our unpublished data) have not provided any evidence for alternate mRNA splicing. There is only a single AATAAA polyadenylation consensus sequence in the 3′ noncoding region (Fig. 1). However, the sequence AATAAG appears at position 989 and might possibly serve as an alternate polyadenylation signal.

Cellular Distribution of the hCD40-L. RNA was obtained from CD3 mAb-stimulated PB T cells and a number of cell lines of myeloid, lymphoid, fibroblastic, and epithelial origin, and examined for hCD40-L transcripts. The following cell types were found negative by Northern blot analysis using 5 μg poly(A)$^+$ RNA per lane: Blin, CB23, Raji, Jurkat, PBM, monocytes, Thp-1, U937, HeLa, A549, placenta, and dermal fibroblasts. After hybridization with the ^{32}P-labeled antisense probe described above, no hCD40-L-specific mRNA could be detected in any cell type other than T cells or their derivatives. In addition, we examined a commercially available Northern blot containing total RNA derived from a variety of human tissues (Fig. 4). On this blot, the radiolabeled hCD40-L probe hybridized with RNA derived from lung tissue. This was somewhat surprising based on the Northern blot analysis of specific cell RNAs. However, it was possible that the hCD40-L-specific mRNA in this lung sample was due to contaminating T lymphocytes. To address this, we rehybridized this tissue blot with a ^{32}P-labeled antisense probe derived from the δ chain of the TCR (Fig. 4 *B*). This experiment resulted in the detection of a band of the expected size which was present exclusively in the lung-derived sample. Therefore, it appears that within the cell types examined thus far, expression of the hCD40-L is restricted to T lymphocytes.

Induction of hCD40-L on PB T Cells. The induction of hCD40-L expression on PB T cells was examined over 36 h after activation with CD3 antibody, PMA, or a combina-

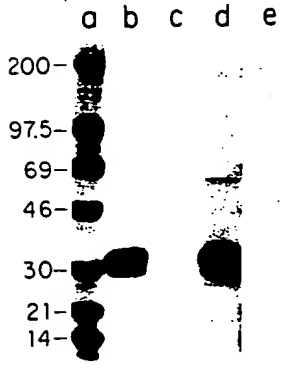

Figure 2. Precipitation of hCD40-L protein using soluble CD40.Fc. COS cells expressing the hCD40-L protein or CD3 mAb-stimulated PB T cells were radiolabeled as described in Materials and Methods. Lysates were precipitated using CD40.Fc and protein A-Sepharose and analyzed under reducing conditions on an 8–16% polyacrylamide SDS gradient gel. Lanes: (*a*) molecular weight markers; (*b*) recombinant hCD40-L protein derived from transfected cells; (*c*) cells transfected with empty vector; (*d*) hCD40-L protein from stimulated PB T cells; and (*e*) unstimulated PB T cells.

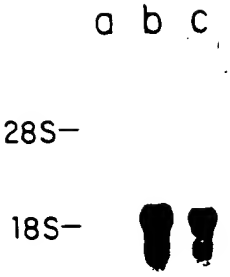

Figure 3. Northern blot analysis of hCD40-L-expressing T cells. Total RNA from stimulated PB T or tonsil T cells was analyzed on Northern blots using a ^{32}P-labeled antisense hCD40-L probe. Lanes: (*a*) unstimulated PB T cells; (*b*) CD3-stimulated PB T cells; and (*c*) PMA plus Con A-stimulated tonsil T cells.

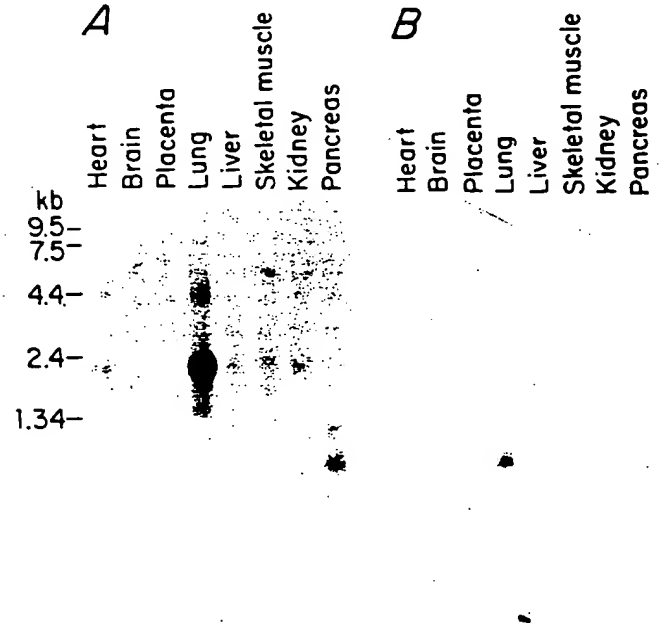

Figure 4. Northern blot analysis of tissue-specific RNAs. Poly(A)$^+$ RNA from the indicated tissues was hybridized with antisense riboprobes as described in Materials and Methods. (*A*) Northern blot hybridized with a radiolabeled probe corresponding to the coding region of the hCD40-L. (*B*) The same Northern blot, partially stripped and rehybridized with a probe specific for the δ chain of the TCR.

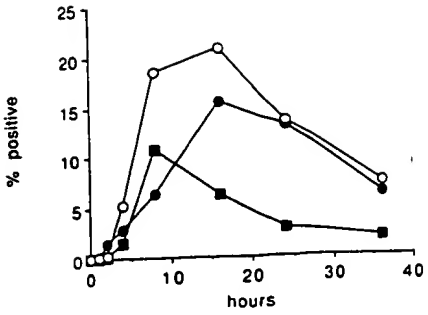

Figure 5. Induction of CD40 ligand expression on PB T cells. Purified peripheral blood T cells were activated for up to 36 h in the presence of 5 μg/ml immobilized CD3 mAb (●), 5 ng/ml PMA (■), or a combination of CD3 mAb plus PMA (○). Cells were harvested at the time indicated, stained with 5 μg/ml biotinylated CD40.Fc and streptavidin-PE, and analyzed by flow cytometry. Results are expressed as the percent of cells positive for biotinylated CD40.Fc binding compared to cells stained with control biotinylated IL-4R.Fc.

tion of the two (Fig. 5). Unstimulated T cells expressed virtually undetectable levels of hCD40-L, as determined by flow cytometric analysis of cells stained with biotinylated CD40.Fc. Treatment with CD3 mAb induced detectable hCD40-L by 4 h, with maximal expression at 8–16 h, and with significant expression still detected at 36 h. Stimulation with PMA resulted in lower levels of ligand expression but similar kinetics of induction. A combination of CD3 mAb and PMA induced detectable hCD40-L by 2 h and resulted in a higher level of ligand expression at 16 h than seen with either factor alone. In contrast to CD3 mAb, PHA alone was not an effective inducer of hCD40-L, but in combination with PMA resulted in levels of ligand comparable to those seen with a combination of CD3 mAb and PMA (data not shown).

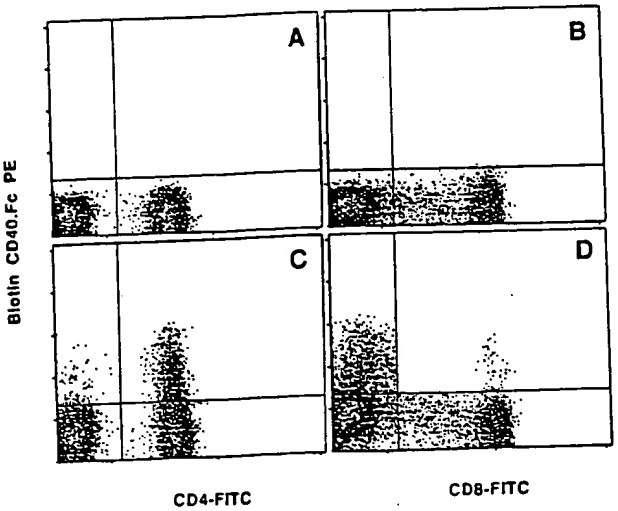

Figure 6. CD40 ligand is induced predominantly on CD4⁺ T cells. Purified PB T cells were cultured for 16 h in medium (*A* and *B*) or activated with 5 μg/ml immobilized CD3 mAb (*C* and *D*) and stained with biotinylated CD40.Fc and streptavidin-PE and either FITC-conjugated CD4 (*A* and *C*) or CD8 (*B* and *D*) mAb. Results are representative from one of six experiments performed.

Expression of hCD40-L on T Cell Subpopulations. CD4⁺ and CD8⁺ PB T cells were examined for the expression of hCD40-L after 18-h stimulation with CD3 mAb (Fig. 6). In the absence of stimulation, CD4⁺ and CD8⁺ T cells expressed no detectable hCD40-L as determined by binding of biotinylated CD40.Fc (Fig. 6, *A* and *B*). After treatment with CD3 mAb, hCD40-L expression was detected primarily on the CD4⁺ population (Fig. 6 *C*). However, a reproducible finding from experiments performed on T cells from many donors was that a small proportion of CD8⁺ T cells was also induced to express hCD40-L (Fig. 6 *D*), although this expression was consistently lower than that seen on CD4⁺ cells.

Induction of Proliferation with CD40-L. The human and murine CD40-L were compared for their ability to mediate B cell proliferation. Purified human tonsil B cells were induced to proliferate in the absence of added cytokines when cultured with fixed CV1/EBNA cells transfected with either human or murine CD40-L (Fig. 7 *A*). This effect appeared to be dose dependent. Addition of IL-4 to cultures enhanced the proliferative response of human B cells to both human and murine ligand.

The effects of hCD40-L on proliferation of murine splenic B cells was also examined (Fig. 7 *B*). As shown previously, mCD40-L was mitogenic in a dose-dependent manner for murine B cells cultured in the absence of costimulus (14). In contrast, under the same culture conditions, CV1/EBNA cells expressing the hCD40-L had virtually no effect. However, the addition of IL-4 to cultures containing the hCD40-L resulted in the proliferation of murine B cells. Although IL-4

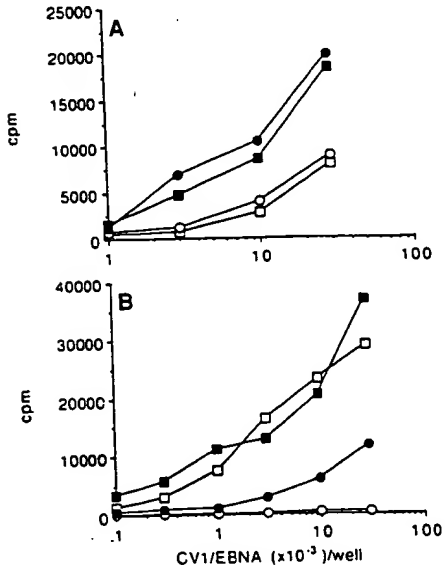

Figure 7. Comparative proliferative responses of B cells to human and murine CD40 ligand. (*A*) 10^5 purified human tonsil B cells were cultured for 6 d with a titration of CV1/EBNA cells transfected with human (●, ○) or murine (■, □) CD40 ligand, in the presence (*filled symbols*) or absence (*open symbols*) of 5 ng/ml hIL-4. (*B*) 10^5 purified murine splenic B cells were cultured for 3 d with CD40 ligand as described above in the presence or absence of 10 ng/ml mIL-4. Results are expressed as mean incorporated cpm from triplicate cultures.

enhanced the response of human B cells to mCD40-L (Fig. 7 *A*), no such enhancement was observed when IL-4 was added to murine B cell cultures containing mCD40-L (Fig. 7 *B*). In both human and murine proliferation assays, CV1/EBNA cells transfected with vector alone had no effect (13, data not shown).

The two forms of CD40-L were compared for their ability to induce IgE secretion from IL-4–activated B cells. Human and murine CD40-L showed comparable activity in the induction of human IgE secretion from purified tonsil B cells (Fig. 8 *A*). As was seen in the proliferation assays, this effect also appeared dose dependent. Similarly, both human and murine forms of CD40-L induced IgE from IL-4–stimulated murine splenic B cells (Fig. 7 *B*), although the human ligand appeared to exhibit lower activity than the murine ligand in this assay. No secreted human or murine IgE was detected in the absence of IL-4 or if CV1/EBNA cells transfected with vector alone were used (14, data not shown).

Discussion

Cell surface molecules expressed on activated T cells that provide contact-dependent help to B cells have been the subject of intense investigation. Recently, a molecule expressed on CD3-activated murine T cells that induces B cells to proliferate in the absence of a costimulus and stimulates IgE secretion from IL-4–activated B cells was cloned and identified as a murine ligand for CD40 (14). Using crosshybridization techniques, we have isolated a human ligand for CD40 that exhibits significant homology (78% identity at the amino acid and 83% at the nucleotide levels) to its murine counterpart. This level of homology suggested that the hCD40-L would be active on both murine and human B cells in a manner similar to that described for mCD40-L (14). In terms of IgE secretion, this was indeed the case, although the hCD40-L displayed lower potency than the mCD40-L on murine B cells. However, with regard to induction of proliferation, we report significant differences between the murine and human CD40-L. Using murine B cells, hCD40-L requires IL-4 for induction of proliferation, whereas mCD40-L does not. On the other hand, in the human B cell culture system both hCD40-L and mCD40-L are capable of inducing significant proliferation in the absence of IL-4. Moreover, IL-4 augments the response of human B cells to hCD40-L and mCD40-L.

Experiments performed in our laboratory (unpublished data) indicate that human and murine B cells differ in the time at which the maximum proliferative response to either hCD40-L or mCD40-L is observed. In murine B cell cultures, the maximal proliferative response is seen at day 2, whereas human B cells show the highest rate of proliferation at day 5, regardless of whether hCD40-L or mCD40-L is used as a stimulus. Because hCD40-L and mCD40-L have comparable activity on human B cells, the inability of hCD40-L to induce the proliferation of murine B cells in the absence of IL-4 is intriguing. One possible explanation for this disparity could be a decreased affinity of hCD40-L compared to mCD40-L for murine CD40.

The predicted amino acid sequence for the murine CD40 molecule is 62% identical to the human CD40 (2). This level of homology might suggest that the binding of both mCD40-L and hCD40-L to either form of CD40 would be comparable. In support of this, we have previously shown that mCD40-L binds to human CD40 with high affinity (21). However, additional binding studies using hCD40-L and mCD40-L will be necessary to further define this interaction.

Another possible explanation for the disparity in the activity of the two ligands is that hCD40-L may not induce proliferation of murine B cells in the absence of costimulus unless the CD40 receptor molecule is being expressed at some required threshold level. It is known that CD40 is constitutively expressed on nonactivated human B cells at high levels relative to those observed on murine B cells (1, 2, 22, and our unpublished observations). The addition of IL-4 to activated murine B cells enhances CD40 mRNA expression (2), which could result in an increased surface expression sufficient to allow the observed proliferative effects. Human B cells also respond to IL-4 by upregulating CD40 expression. However, if a minimum number or relative density of CD40 is required for optimal signaling, the comparable activity of hCD40-L and mCD40-L on human B cells in the absence of IL-4 may simply reflect the increased level of CD40 expression. In contrast to the proliferation assays performed in the absence of a costimulus, the observation that hCD40-L and mCD40-L induce similar levels of IgE from murine B cells is likely due to the absolute requirement for IL-4 in secretion of this isotype.

The conformation of the ligands and the CD40 receptors no doubt play an important role in defining their relative

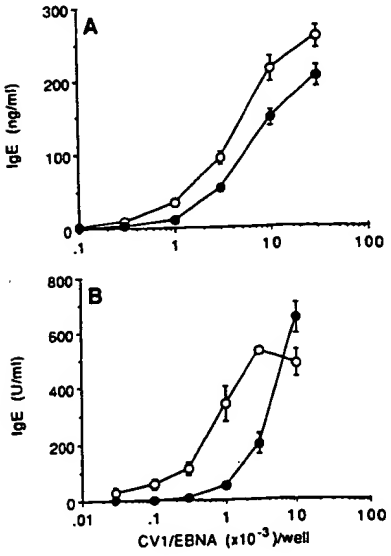

Figure 8. Human and murine IgE secretion induced by CD40 ligand. (*A*) 10^5 purified human tonsil B cells were cultured for 10 d with a titration of CV1/EBNA cells transfected with human (●) or murine (○) CD40 ligand, in the presence of 5 ng/ml hIL-4. (*B*) 10^5 purified murine splenic B cells were cultured for 7 d with CD40 ligand as described above in the presence of 10 ng/ml mIL-4. Results are expressed as mean values ± SEM from triplicate cultures.

affinities for one another. Fine structure epitope mapping using panels of mAbs will be useful, however, as of yet, such reagents are unavailable. Recently, Lederman et al. (23) described a mAb directed against a 30-kD activated T cell surface antigen which resembles the hCD40-L in its functional effects. This antibody inhibits the B cell proliferation and CD23 expression induced by activated $CD4^+$ T cells. However, the kinetics of induction of the T cell surface antigen recognized by this antibody differ from that seen in our laboratory for the hCD40-L. In addition, reactivity of this antibody is restricted to $CD4^+$ T cells, whereas hCD40-L can also be induced on a small percentage of $CD8^+$ T cells. Further studies will be necessary to determine the exact identity of the T cell antigen recognized by this antibody and its relationship to the hCD40-L.

The significance of the induction of the hCD40-L on a small proportion of $CD8^+$ PB T cells is unclear. Attempts to induce the expression of hCD40-L on human T cell clones (our unpublished observations) have thus far been successful only in $CD4^+$ cells, despite the fact that several $CD8^+$ clones have also been examined. Studies are currently underway to determine whether $CD8^+$ cells expressing hCD40-L play a unique role in the normal immune response in vivo.

In addition to B cells, the cellular distribution of CD40 includes follicular dendritic cells and epithelial cells. Given the diversity of the response to B cells to the CD40-L, it will be of interest in the future to determine the role of the CD40-L in the biology of other cell types.

The authors wish to thank Steve Gimpel for sequencing the cDNA; Ken Grabstein and David Cosman for helpful discussions; and Anne C. Bannister for editorial assistance.

Address correspondence to Dr. Melanie K. Spriggs, Immunex R & D Corporation, 51 University Street, Seattle, WA 98101.

Received for publication 30 July 1992.

References

1. Stamenkovic, I., E.A. Clark, and B. Seed. 1989. A B-lymphocyte activation molecule related to the nerve growth factor receptor and induced by cytokines in carcinomas. *EMBO (Eur. Mol. Biol. Organ.) J.* 8:1403.
2. Torres, R.M., and E.A. Clark. 1992. Differential increase of an alternatively polyadenylated mRNA species of murine CD40 upon B lymphocyte activation. *J. Immunol.* 148:620.
3. Smith, C.A., T. Davis, D. Anderson, L. Solam, M.P. Beckmann, R. Jerzy, S.K. Dower, D. Cosman, and R.G. Goodwin. 1990. A receptor for tumor necrosis factor defines an unusual family of cellular and viral proteins. *Science (Wash. DC).* 248:1019.
4. Dürkop, H., U. Latza, M. Hummel, F. Eitelbach, B. Seed, and H. Stein. 1992. Molecular cloning and expression of a new member of the nerve growth factor receptor family that is characteristic for Hodgkin's disease. *Cell.* 68:421.
5. Clark, E.A., and J.A. Ledbetter. 1986. Activation of human B cells mediated through two distinct cell surface differentiation antigens, Bp35 and Bp50. *Proc. Natl. Acad. Sci. USA.* 83:4494.
6. Paulie, S., A. Rosen, B. Ehlin-Henriksson, S. Braesch-Andersen, E. Jakobsen, H. Koho, and P. Perlmann. 1989. The human B lymphocyte and carcinoma antigen, CDw40, is a phosphoprotein involved in growth signal transduction. *J. Immunol.* 142:590.
7. Banchereau, J., P. de Paoli, A. Valle, E. Garcia, and F. Rousset. 1991. Long term human B cell lines dependent on interleukin-4 and antibody to CD40. *Science (Wash. DC).* 251:70.
8. Jabara, H.H., S.M. Fu, R.S. Geha, and D. Vercelli. 1990. CD40 and IgE: synergism between anti-CD40 monoclonal antibody and interleukin 6 in the induction of IgE synthesis by highly purified human B cells. *J. Exp. Med.* 172:1861.
9. Zhang, K., E.A. Clark, and A. Saxon. 1991. CD40 stimulation provides an IFN-gamma-independent and IL-4–dependent differentiation directly to human B cells for IgE production. *J. Immunol.* 146:1836.
10. Valle, A., C.E. Zuber, T. Defrance, O. Djossou, M. DeRie, and J. Banchereau. 1989. Activation of human B lymphocytes through CD40 and interleukin 4. *Eur. J. Immunol.* 19:1463.
11. Barrett, T.B., G. Shu, and E.A. Clark. 1991. CD40 signaling activates CD11a/CD18 (LFA-1)-mediated adhesion in B cells. *J. Immunol.* 146:1722.
12. Uckun, F.M., G.L. Schieven, I. Diberdik, M. Chandan-Langlie, L. Tuel-Ahlgren, and J.A. Ledbetter. 1991. Stimulation of protein tyrosine phosphorylation, phosophoinositide turnover, and multiple previously unidentified serine/threonine-specific protein kinases by the pan-B-cell receptor CD40/Bp50 at discrete developmental stages of human B-cell ontogeny. *J. Biol. Chem.* 266:17478.
13. Liu, Y.J., D.E. Joshua, G.T. Williams, C.A. Smith, J. Gordon, and I.C.M. MacLennon. 1989. Mechanism of antigen-driven selection in germinal centres. *Nature (Lond.).* 342:929.
14. Armitage, R.J., W.C. Fanslow, L. Strockbine, T.A. Sato, K.N. Clifford, B.M. Macduff, D.M. Anderson, S.D. Gimpel, T. Davis-Smith, C.R. Maliszewski, et al. 1992. Molecular and biological characterization of a murine ligand for CD40. *Nature (Lond.).* 357:80.
15. Widmer, M.B., R.B. Acres, H.M. Sassenfeld, and K.H. Grabstein. 1987. Regulation of cytolytic cell populations from human peripheral blood by B cell stimulatory factor 1 (interleukin 4). *J. Exp. Med.* 166:1447.
16. Fanslow, W.C., D. Anderson, K.H. Grabstein, E.A. Clark, D. Cosman, and R.J. Armitage. 1992. Soluble forms of CD40 inhibit biological responses of human B cells. *J. Immunol.*

149:655.
17. Mosley, B., M.P. Beckmann, C.J. March, R.L. Idzerda, S.D. Gimpel, T. VandenBos, D. Friend, A. Alpert, D. Anderson, J. Jackson, et al. 1989. The murine interleukin-4 receptor: molecular cloning and characterization of secreted and membrane bound forms. *Cell.* 59:355.
18. McMahan, C.J., J.L. Slack, B. Mosley, D. Cosman, S.D. Lupton, L.L. Brunton, C.E. Grubin, J.M. Wignall, N.A. Jenkins, C.I. Brannan, et al. 1991. A novel IL-1 receptor, cloned from B cells by mammalian expression, is expressed in many cell types. *EMBO (Eur. Mol. Biol. Organ.) J.* 10:2821.
19. Southern, P.J., and P. Berg. 1982. Transformation of mammalian cells to antibiotic resistance with a bacterial gene under control of the SV40 early region promoter. *J. Mol. Appl. Genet.* 1:327.
20. Spriggs, M.K., P.J. Lioubin, J. Slack, S.K. Dower, U. Jonas, D. Cosman, J.E. Sims, and J. Bauer. 1990. Induction of IL-1 receptor (IL-1R) on monocytic cells. Evidence that the IL-1 receptor is not encoded by a T-cell type IL-1 receptor message. *J. Biol. Chem.* 265:22499.
21. Armitage, R.J., T. Sato, B.M. Macduff, K. Clifford, A. Alpert, C.A. Smith, and W.C. Fanslow. 1992. Identification of a source of biologically active CD40 ligand. *Eur. J. Immunol.* 22:2071.
22. McMichael, A., P.C.L. Beverley, S. Cobbold, M.J. Crumpton, W. Gilks, F.M. Gotch, N. Hogg, M. Horton, N. Ling, I.C.M. MacLennan, et al., editors. 1987. Leucocyte Typing III. Oxford University Press, Eynsham, Oxon.
23. Lederman, S., M.J. Yellin, A. Krichevsky, J. Belko, J.J. Lee, and L. Chess. 1992. Identification of a novel surface protein on activated CD4$^+$ T cells that induces contact-dependent B cell differentiation (Help). *J. Exp. Med.* 175:1091.

APPENDIX D

Figure 1 – Juswinder Singh Declaration B189

```
1cda: GDEDPQIAAHVVSEANSNAASVLQWAKKGYYTMKSNLVML
1aly: GDQNPQIAAHVISEASSKTTSVLQWAEKGYYTMSNNLVTL

1cda: ENGKQLTVKREGLYYVYTQVTFCSNREPSSQRPFIVGLWL
1aly: ENGKQLTVKRQGLYYIYAQVTFCSNREASSQAPFIASLCL

1cda: KPSIGSERILLKAANTHSSSQLCEQQSVHLGGVFELQAGA
1aly: KSPGRFERILLRAANTHSSAKPCGQQSIHLGGVFELQPGA

1cda: SVFVNVTEASQVIHRVGFSSFGLLKL
1aly: SVFVNVTDPSQVSHGTGFTSFGLLKL
```

Amino acid sequence alignment between amino acid residues Gly116 to Leu261 of the crystal structure model of human CD40L (1aly) in the present application and the corresponding amino acid residues in the Peitsch model of mouse CD40L (1cda).

APPENDIX E

Communication

THE JOURNAL OF BIOLOGICAL CHEMISTRY
Vol. 267, No. 4, Issue of February 5, pp. 2119-2122, 1992

The Structure of Human Lymphotoxin (Tumor Necrosis Factor-β) at 1.9-Å Resolution*

(Received for publication, August 16, 1991)

Michael J. Eck‡‖, Mark Ultsch§, Ernst Rinderknecht§, Abraham M. de Vos§, and Stephen R. Sprang‡¶

From the ‡Howard Hughes Medical Institute and Department of Biochemistry, The University of Texas Southwestern Medical Center, Dallas, Texas 75235-9050 and §Genentech, Inc., South San Francisco, California 94080

The three-dimensional structure of recombinant human lymphotoxin (residues 24–171 of the mature protein) has been determined by x-ray crystallography at 1.9-Å resolution (R_{cryst} = 0.215 for $I > 3\sigma_{(I)}$). Phases were derived by molecular replacement using tumor necrosis factor (TNF-α) as a search model.

Like TNF-α, lymphotoxin (LT) folds to form a "jellyroll" β-sheet sandwich. Three-fold related LT subunits form a trimer stabilized primarily by hydrophobic interactions. A cluster of 6 basic residues around the 3-fold axis may account for the acid lability of the trimer.

Although the structural cores of TNF-α and LT are similar, insertions and deletions relative to TNF-α occur in loops at the "top" of the LT trimer and significantly alter the local structure and the overall shape of the molecule. The structure of the "base" of the trimer is highly conserved. The sites of two mutations (Asp-50 and Tyr-108) that abolish the cytotoxicity of LT are contained within poorly ordered loops of polypeptide chain that flank the cleft between neighboring subunits at the base of the molecule, suggesting that the receptor recognizes an intersubunit binding site.

Lymphotoxin (LT,[1] also called tumor necrosis factor-β) is a lymphocyte-secreted cytokine 32% identical in primary sequence to monocyte/macrophage-derived tumor necrosis factor-α (TNF-α) (1, 2). LT exhibits pleiotropic activities very similar to those of TNF-α. Both molecules are cytotoxic to a variety of tumor cell lines *in vitro* and can induce hemorrhagic necrosis of tumors *in vivo* (3). Similarly, LT mediates proinflammatory (4) and antiviral (5) responses and alters the proliferative state of a variety of cell types (1). Both TNF-α and LT bind to each of two distinct TNF receptors (6–8), but their relative affinities have not been well studied. In contrast, the cellular origins, mechanism of induction, and mode of secretion of LT and TNF-α are different (1), and the two cytokines produce different effects on several lymphoid, endothelial, and other cellular targets (9). Unlike human TNF-α, human LT is a glycoprotein, contains no disulfide bonds (3), and is unstable in the presence of acid, detergents, and organic solvents.

Because the three-dimensional structures of LT and TNF-α are key to understanding the differences in their biological and physical properties, we have undertaken crystallographic analysis of both molecules. We (10) and others (11) have reported the structure of TNF-α. Here we describe the 1.9-Å resolution structure of a truncated, active, recombinant, and non-glycosylated form of human lymphotoxin corresponding to residues 24–171 of the mature LT found *in vivo*.

EXPERIMENTAL PROCEDURES

Recombinant human lymphotoxin (residues 24–171) was expressed in *Escherichia coli* and purified as described previously (3). Crystals were grown by vapor diffusion at 4 °C from hanging drops containing 0.5 M NaCl, 20 mM Tris, pH 8.0, and 4 mg/ml protein over well solutions containing 40% saturated NaCl. Crystals of space group R32 (Table I) grew as thin hexagonal plates as large as 0.5 mm across and 0.08 mm thick.

Diffraction data were recorded from two native crystals using a Xuong/Hamlin-type multiwire area detector system (12). Graphite monochromated CuKα x-rays were produced by a Rigaku RU-200 generator operating at 5.4 kilowatts, and data were measured at 21–25 °C by omega scans at a speed of 0.1 degrees/min. "Shifts" of 5° of data were scaled and merged using the PROTEIN package (13). Individual scale factors were applied to each shift; a single exponential (B) scale factor was applied to all shifts from a single crystal.

Atomic coordinates for monomer "A" from data set 1TNF in the Brookhaven Protein Databank (10, 14) were used as a search model for phase determination by molecular replacement (15). Rotation and translation functions, and crystallographic refinement calculations were carried out using the program package X-PLOR (16).

Cross-rotation function solutions at 3.5 Å, eulerian angles θ_1 = 223.3, θ_2 = 119.4, θ_3 = 61.9 (peak A) and θ_1 = 219.8, θ_2 = 119.5, θ_3 = 18.3 (peak B) (related by a non-crystallographic 2-fold axis that was located in a native 3.5-Å Patterson self-rotation function at polar angles ϕ = 0.0, Ψ = 22.5, K = 180.0, 7.5° away from the hexagonal x axis in the xy plane) were refined by Patterson correlation (17). Peak A was the largest (3.8 S.D. above the mean) in a rotation function calculated over the asymmetric unit at 4.5-Å resolution using vector lengths from 5 to 25 Å and a 2.5° step size. Peak B was not among the 6000 highest peaks in this map but was located in a second rotation function calculated in 1.0° increments over a limited angular range (Φ_1 = 220.0 − 225.0°, Φ_2 = 115.0 − 122.5°, Φ_3 = 0.0 − 70.0°) using vectors from 15 to 25 Å in length.

Two $E_{obs}{}^*E^2_{calc}$ translation function solutions (both 7 S.D. over the mean with data to 3.5-Å resolution), each corresponding to one of the two rotation function solutions, generated TNF-like trimers by crystallographic symmetry. Rigid body least squares minimization of $(F_{calc} - F_{obs})^2$ yielded a crystallographic R value of 0.51 for data to 3.5-Å resolution.

At this stage the model was rebuilt to reflect the amino acid sequence of LT (3). Model building and least squares superpositions were performed with the graphics program "O" (18). Five cycles of simulated annealing refinement (19) excluding non-crystallographic symmetry restraints after the first cycle, followed by manual inspection and rebuilding, were performed at resolutions of 2.5, 2.5, 2.25, 2.25, and finally 1.9 Å. Residues 24–32, 34–41, 39–46, 46–54, 84–91, 89–96, 99–103, 104–110, 110–117, 122–129, 158–165, and 168–171 were refit into simulated annealing omit maps (16) calculated at 2.25-

---

* Atomic coordinates have been submitted to the Protein Data Bank at Brookhaven National Laboratory for release 6 months after date of publication. The costs of publication of this article were defrayed in part by the payment of page charges. This article must therefore be hereby marked "*advertisement*" in accordance with 18 U.S.C. Section 1734 solely to indicate this fact.

¶ To whom correspondence should be addressed: Howard Hughes Medical Institute, and Dept. of Biochemistry, University of Texas Southwestern Medical Center, 5323 Harry Hines Blvd., Dallas, TX 75235-9050. Tel.: 214-689-5008; Fax: 214-689-5066.

‖ Present address: Children's Hospital, Howard Hughes Medical Institute, 300 Longwood Dr., Boston, MA 02115.

[1] The abbreviations used are: LT, lymphotoxin; TNFα, tumor necrosis factor-α.

TABLE I

Crystallographic data and refinement statistics

Crystal parameters	
Space group	R32
Cell constants (hexagonal setting)	$a = b = 55.86$ $c = 518.86$
Subunits/cell	36
Protein content	51%
Data collection statistics	
No. observations (all)	87,164
Observations, $I > 3\sigma_{(I)}$	52,136
No. unique reflections to 1.9 Å	23,666
R_{merge}[a]	0.068
% complete at 1.9 Å	84.9
% complete 1.95–1.90 Å	67.5
Refinement statistics	
Number of atoms	2298
R_{cryst} (6–1.9 Å), $I > 3\sigma_{(I)}$	0.215
Root mean square deviation from ideal	
Bond lengths	0.014 Å
Bond angles	3.7°

[a] $R_{merge} = \Sigma_h\Sigma_i |I_i(h) - I_i(h)| / \Sigma_h\Sigma_i I_i(h)$ where $I_i(h)$ and $I(h)$ are the ith and the mean measurement of the intensity of reflection h. $R_{cryst} = \Sigma_h ||F_{obs}(h) - F_{calc}(h)| / \Sigma_h F_{obs}(h)|$ where $F_{obs}(h)$ and $F_{calc}(h)$ are the observed and calculated structure factor amplitudes.

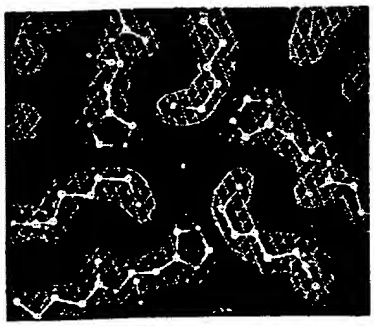

FIG. 1. **A section of the $2F_{obs} - F_{calc}$ electron density map computed with data between 8 and 1.9 Å and phases determined from the refined atomic model and contoured at 1.5 σ units above the mean value of the map.** The view is centered on and parallel to the crystallographic 3-fold axis and shows lysine 119 and histidine 131 of triad-related molecules A. The conformation about the His-131 Cβ-Cγ bond could not be unambiguously determined.

Å resolution. Restrained, individual temperature factors were refined after the last cycle of simulated annealing. No solvent molecules are included in the present model.

Data collection and refinement statistics are summarized in Table I. A portion of the 1.9-Å electron density map is shown in Fig. 1.

Solvent accessible surface areas were computed with software written by T. Richmond based on the algorithm of Lee and Richards (28).

RESULTS AND DISCUSSION

Structure and Comparison to TNF-α—The tertiary fold of lymphotoxin is virtually identical to that of TNF-α (Fig. 2) (10, 11) and comprises a sandwich of two predominantly antiparallel β-pleated sheets of "jellyroll" Greek-key topology (20). The conformations of the β-sheets and of the loops connecting the sheets at the base of the LT subunit (Fig. 2) are very similar to those of the corresponding structures in TNF-α. Superposition of the two molecules using Cα atoms of the β-strand residues only (Fig. 2) yields a root mean square positional deviation of 0.61 Å between the 108 equivalent atoms. On the basis of this superposition, the primary sequences of TNF-α and LT can be aligned as shown in Fig. 3.

The two crystallographically independent molecules of LT in the unit cell are quite similar within the β-sheet (root mean square positional deviation between molecules A and B after superposition of Cα atoms in β-strands defined in Fig. 2 is 0.28 Å) but differ significantly in certain connecting loops. In molecule A the C-D (residues 84–94) and E-F (residues 123–127) loops are well ordered and stabilized by contacts with a symmetry-related molecule while in molecule B they are less well ordered and adopt different conformations. The conformation of the two molecules differs in other segments (A–A', residues 36–40; A'–A'', 48–51; D–E, 105–109) where the polypeptide chain is poorly ordered or poorly defined in the electron density.

Lymphotoxin subunits form trimers similar to those of TNF-α in which the 3-fold axis of the trimer is aligned approximately with the strands of the subunit β-strands. Trimers are assembled such that the "edge" of each subunit β-sandwich (strands E and F) is packed against the inner sheet "face" (strands A, A'', H, C, and F) of its neighbor.

Of the 35 residues that form the hydrophobic core of the β-sandwich in LT, 20 are identical in TNF-α and only 5 are clearly non-conservative replacements. Several substitutions that might be expected to perturb the packing between opposing sheets are compensated by complementary changes in neighboring side chains. For example, the interacting pair of residues Phe-58/Ala-168 in LT are replaced by Val-41/Ile-154 in TNF-α, thus conserving hydrophobicity and volume. Substitution of Ser-117/His-135 in LT by Ala-96/Leu-120 in TNF-α replaces polar residues with a buried hydrophobic pair.

Only 13 of the 80 residues in the LT trimer with a solvent accessible surface area greater than 20 Å^2 are conserved in the primary sequence of TNF-α. The majority are located toward the base of the trimer in the polypeptide loops connecting the β-sheets (Fig. 2). The conserved Tyr-108 projects into the crevice between neighboring subunits.

The C-D loop in LT is 4 residues longer than that in TNF-α, while the E-F loop contains 5 fewer residues (Fig. 2). The longer C-D loop contains 1½ turns of helix and folds compactly across the top of molecule A but is extended and poorly ordered in molecule B. In TNF-α the C-D and E-F loops are connected by a disulfide bridge between Cys-69 and Cys-101. Both of these residues are substituted by tyrosine in human LT, and their Cα atoms are separated by 13 Å. Although both cysteines are present in bovine and rabbit LT (21), they could not be expected to form a disulfide bond (Fig. 2). The C-D loop rolls away from the axis of the TNF trimer and, with the deletion in the E-F loop, creates a molecule that is less elongated than the TNF-α trimer and which flares open at the top (Fig. 5). The G-H loop in LT contains one fewer residue than that in TNF-α, but only local conformational differences are observed.

The lymphotoxin trimer is stabilized primarily by interactions between hydrophobic and aromatic side chains. Six aromatic residues and one histidine are present on the surface of the inner "face" sheet formed by strands A'', A, H, C, and F (Fig. 4). Intervening glycine residues allow the aromatic residues to pack flat against the surface formed by the main chain atoms. This "aromatic tiling" is not as prominent in TNF-α, where the 3 phenylalanine residues nearest the base of the trimer are replaced by leucine or isoleucine. Three of the aromatic residues (Phe-74, Tyr-134, and Phe-169) pack around the trimer 3-fold axis.

At the top and bottom of the trimer, the subunit interface is characterized by charged and polar interactions. As in TNF-α, Lys-28 near the amino terminus forms a salt bridge with

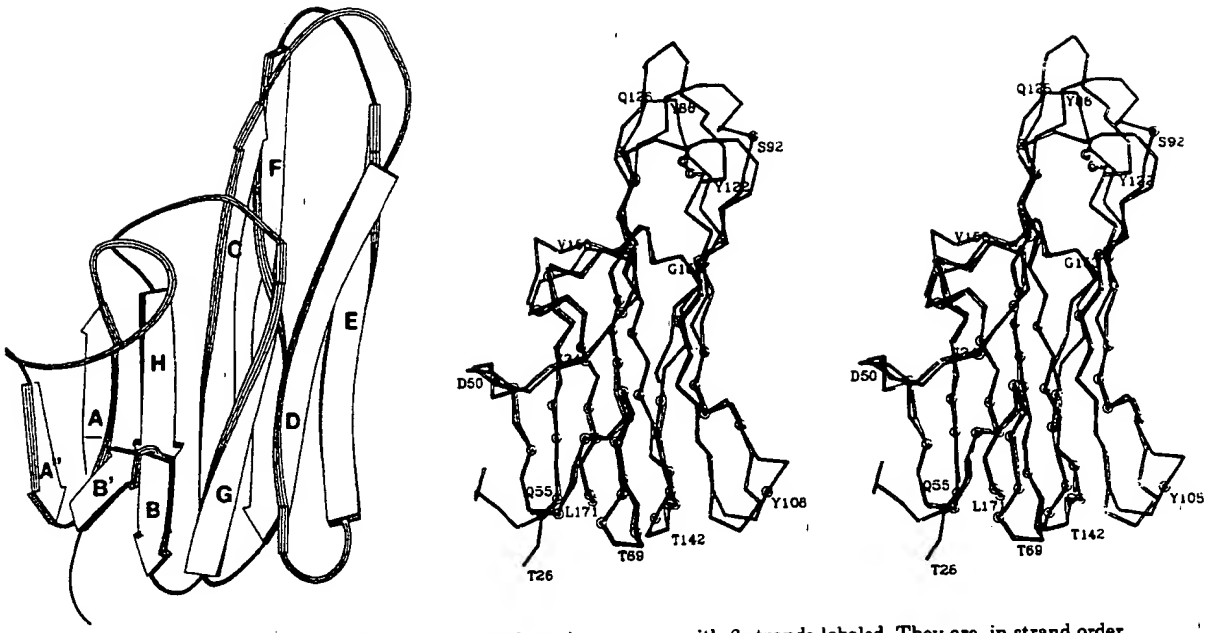

FIG. 2. *Left*, a ribbon tracing (27) the lymphotoxin monomer with β-strands labeled. They are, in strand order for the inner sheet facing the trimer axis: strand A'', residues 52–56; A, 28–35; H, 164–169; C, 72–84; F, 127–140. Strands in the outer sheet are: A', 43–47 (not shown); B', 58–62; B, 64–68; G, 144–152; D, 93–105; E, 111–122. *Right*, least squares superposition of Cα atoms of molecule A of lymphotoxin onto corresponding atoms of TNF-α (10) (molecule A of 1TNF from the Protein Databank (14)). Tyrosines 86 and 122 in LT correspond to cystines 69 and 101 which form a disulfide bridge in TNF-α. Cα atoms shown with *large spheres* mark identically conserved residues in TNF-α and LT.

```
                    |1          |9
                    VRSSSRTP    SDKPVAHVVANPQAEGQLQWLNRRA   TNF
                    ........    ..KP.AH....P.....L.W.....   Con
LPGVGLTPSAAQTARQHPKMHLAHS       TLKPAAHLIGDPSKQNSLLWRANTD   LT
|1                              |26

|34                            |59
NALLANGVELRDNQLVVPSEGLYLI       YSQVLFKGQGCP----STHVLLTHT   TNF
.A.L..G..L..N.L.VP..G.Y..       YSQV.F.G........S....L.H.   Con
RAFLQDGFSLSNNSLLVPTSGIYFV       YSQVVFSGKAYSPKATSSPLYLAHE   LT
|51                            |76

|80                            |105
ISRIAVSYQTKVNLLSAIKSPCQRE       TPEGAEAKPWYEPIYLGGVFQLEKG   TNF
.......Y...V.LLS..K......       ........PW....Y.G..FQL..G   Con
VQLFSSQYPFHVPLLSSQKMVYP--       ----GLQEPWLHSMYHGAAFQLTQG   LT
|101                                 |124

|130                           |155
DRLSAEINRPDYLDFAESGQVYFGI       IAL  TNF
D.LS.........L....S..V.FG.      .AL  Con
DQLSTHTDGIPHLVLSPS-TVFFGA       FAL  LT
|145                           |169
```

FIG. 3. **Primary sequence alignment of human LT (*LT*) and TNF-α (*TNF*) based on the best structural superposition determined in program "O" (18).** Fifty of the 157 residues (32%) in TNF-α are identically conserved (*Con*) in lymphotoxin.

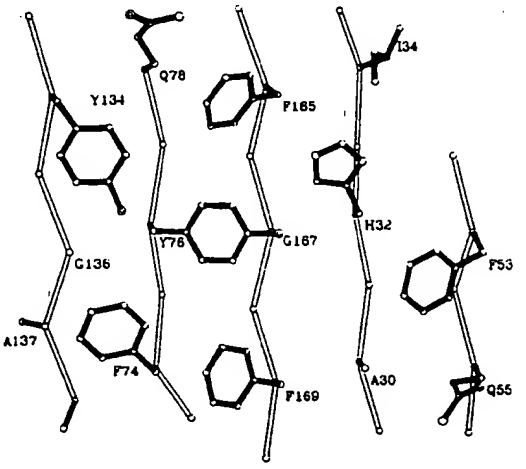

FIG. 4. **The inner "face" of the LT monomer is tiled with aromatic residues.** This surface packs against the "edge" of an adjacent subunit in the trimer, forming the hydrophobic core of the molecule. All side chains on this surface which project into the trimer interface are shown.

the carboxylate of the COOH terminus of the adjacent subunit, forming a ring of ion pair interactions around the 3-fold axis. Near the top of the trimer, Lys-119 and His-131 from each subunit form a cluster around the 3-fold axis (Fig. 1). The Nϵ atoms of Lys-119 are mutually separated by 5.4 Å but are located within 4 Å of the carbonyl oxygen of Leu-130 and the imidazole ring of His-131. Interactions with these groups and with a network of solvent molecules provide the only source of charge compensation for the lysine residues. On protonation, the histidine residues would contribute, together with lysines 119, six formal positive charges to the trimer interface, possibly accounting for the acid lability of LT. In contrast, in the more acid-stable TNF-α, His-131 is replaced by a glutamic acid residue which forms a neutralizing ion pair with Lys-98, the counterpart to Lys-119 in LT.

Site of Receptor Binding—Goh *et al.* (22) have shown that LT mutants with single amino acid substitutions at either Asp-50 or Tyr-108 have greatly reduced receptor binding and cytotoxic activity. These residues are contained within poorly ordered solvent-accessible loops (connecting strands A'–A'' and D–E, respectively) that flank the interface between subunits in the trimer but do not participate in intersubunit contacts (Fig. 5). On the basis of this result and comparable results from mutagenic analysis of TNF-α (23, 24), it has been proposed (22, 23) that the receptor binds to TNF-α and LT in the cleft between subunits near the base of the trimer, which has been shown to be the active species (25). The flexibility of these loops in LT and TNF-α (10) might allow

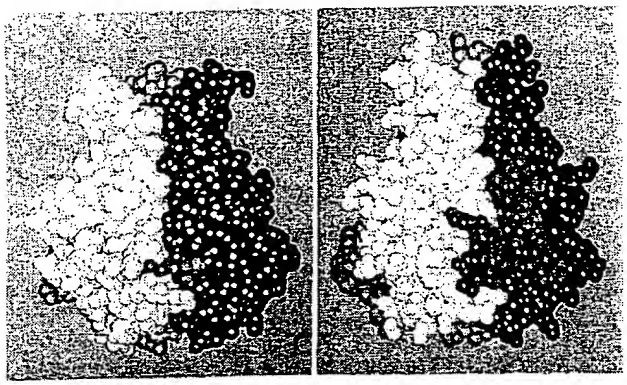

FIG. 5. **van der Waals surface of the lymphotoxin (*left*) and TNF-α (*right*) trimers.** Subunits are colored *white*, *gray*, and *charcoal*. Mutagenic "hot spots," associated with changes in cytotoxicity or receptor binding, are shown in *red*. On LT, these are Tyr-108 (on *white* subunit) and Asp-50 (on *black* subunit) (22). In TNF-α, mutagenesis of residues 84–91 (on *white* subunit), 30–34 (lower group on *charcoal* subunit), and 143–149 (upper group on *charcoal* subunit) can alter cytotoxicity (21, 23, 24).

structural adaptation to the binding surfaces of the two different receptors. The lack of sequence homology between TNF-α and LT in this region may indicate that the two cytokines employ alternative receptor binding conformations. Potentially, three receptors could simultaneously interact with a LT or TNF-α trimer, providing a mechanism for ligand-induced receptor aggregation (10, 21–23), which has been shown to mediate cytotoxicity in L-929 cells (26).

A region at the base of the TNF-α trimer, contiguous with the surface formed by the loops described above, has also been proposed to form part of the receptor binding surface (10). The structure and primary sequence of the A''–B, B'–B, B–C, and F–G loops are well conserved in TNF-α and LT. Conserved residues Pro-37, Gly-57, Gly-71, and Gly-144 maintain the conformation of the polypeptide turns, and leucines 54 and 60 could provide a hydrophobic receptor binding surface. Most mutations in these segments produce unstable, inactive molecules (24), which suggest that residues at these sites stabilize the tertiary or quaternary structure, but this does not exclude their involvement in receptor binding. A definitive description of LT-receptor interactions must await direct structural studies of the complexes.

Acknowledgments—We thank Dr. Anthony Kossiakoff for his continuing support of this project and Dr. Elizabeth Goldsmith for critically reading the manuscript.

REFERENCES

1. Paul, N. L., and Ruddle, N. H. (1988) *Annu. Rev. Immunol.* **38**, 407–438
2. Pennica, D., Nedwin, G. E., Hayflick, J. S., Seeburg, P. H., Derynck, R., Palladino, M. A., Kohr, W. J., Aggarwal, B. B., and Goeddel, D. V. (1984) *Nature* **312**, 724–729
3. Gray, P. W., Aggarwal, B. B., Benton, C. V., Bringman, T. S., Henzel, W. J., Jarrett, J. A., Leung, D. W., Moffat, B., Ng, P., Svedersky, L. P., Palladino, M. A., and Nedwin, G. E. (1984) *Nature* **312**, 721–724
4. Shalaby, M. R., Aggarwal, B. B., Rinderknecht, E., Svedersky, L. P., Finkle, B. S., and Palladino, M. R., Jr. (1985) *J. Immunol.* **135**, 2069–2073
5. Wong, G. H. W., and Goeddel, D. V. (1986) *Nature* **323**, 819–822
6. Loetscher, H., Pan, Yu-C. E., Lahm, H.-W., Gentz, R., Brockhaus, M., Tabuchi, H., and Lesslauer, W. (1990) *Cell* **61**, 351–359
7. Schall, T. J., Lewis, M., Koller, K. J., Lee, A., Rice, G. C., Wong, G. H. W., Gatanaga, T., Granger, G. A., Lentz, R., Raab, H., Kohr, W. J., and Goeddel, D. V. (1990) *Cell* **61**, 361–370
8. Smith, C. A., Davis, T., Anderson, D., Solam, L., Beckmann, M. P., Jerzy, R., Dower, S. K., Cosman, D., and Goodwin, R. G. (1990) *Science* **248**, 1019–1023
9. Aggarwal, B. B. (1990) in *Tumor Necrosis Factor: Structure, Mechanism of Action, Role in Disease and Therapy* (Granger, B. B., ed) pp. 49–54, International Conference on Tumor Necrosis Factor and Related Cytokines, Napa, CA
10. Eck, M. J., and Sprang, S. R. (1989) *J. Biol. Chem.* **264**, 17595–17605
11. Jones, E. Y., Stuart, D. I., and Walker, N. P. C. (1989) *Nature* **338**, 225–228
12. Hamlin, R., Cork, C., Howard, A., Nielsen, C., Vernon, W., Matthews, D., and Xuong, N.-H. (1981) *J. Appl. Crystallogr.* **14**, 85–93
13. Steigemann, W. (1989) *PROTEIN, A Program System for the Crystal Structure Analysis of Proteins*, Max-Planck-Institut für Biochemie, Martinsried bei Muenchen, Federal Republic of Germany
14. Bernstein, F. C., Koetzle, T. F., Williams, J. B., Meyer, E. F., Jr., Brice, M. D., Rodgers, J. R., Kennard, O., Shimanouchi, T., and Tasumi, M. (1977) *J. Mol. Biol.* **112**, 535–542
15. Rossmann, M. G. (1972) *The Molecular Replacement Method: A Collection of Papers on the Use of Non-crystallographic Symmetry*, Gordon and Breach, New York
16. Brünger, A. T. (1990) *X-PLOR (Version 2.1) Manual*, Yale University, New Haven, CT
17. Brünger, A. T. (1990) *Acta Crystallogr.* **A46**, 46–57
18. Jones, T. A., and Kjeldgaard, M. (1990) *O Version 5.6*, Department of Molecular Biology, Uppsala University, Uppsala, Sweden
19. Brünger, A. T., Kuriyan, J., and Karplus, M. (1987) *Science* **235**, 458–460
20. Richardson, J. (1981) *Adv. Protein Chem.* **34**, 167–339
21. Sprang, S. R., and Eck, M. J. (1991) in *The Tumor Necrosis Factors: The Molecules and Their Emerging Role in Medicine* (Beutler, B., ed) pp. 11–32, Raven Press, New York
22. Goh, C. R., Loh, C.-S., and Porter, A. G. (1991) *Protein Eng.* **4**, 785–792
23. Van Ostade, X., Tavernier, J., Prangé, T., and Fiers, W. (1991) *EMBO J.* **10**, 827–836
24. Yamagishi, J.-I., Kawashima, H., Matsuo, N., Ohue, M., Yamayoshi, M., Toshikazu, F., Kotani, H., Furuta, R., Nakano, K., and Yamada, M. (1990) *Protein Eng.* **3**, 713–719
25. Smith, R. A., and Baglioni, C. (1987) *J. Biol. Chem.* **262**, 6951–6954
26. Engelmann, H., Holtmann, H., Brakebusch, C., Avni, Y. S., Sarov, I., Nophar, Y., Hadas, E., Leitner, O., and Wallach, D. (1990) *J. Biol. Chem.* **265**, 14497–14504
27. Priestle, J. P. (1988) *J. Appl. Crystallogr.* **21**, 572–576
28. Lee, B., and Richards, F. M. (1971) *J. Mol. Biol.* **55**, 379–400